Geophysical Research Letters

RESEARCH LETTER
10.1029/2025GL118366

Recent Cloud Controlling Factor Analyses Indicate Higher Climate Sensitivity

Sarah Wilson Kemsley[1,2], **Peer Nowack**[3,4], **and Paulo Ceppi**[5]

[1]Climatic Research Unit, School of Environmental Sciences, University of East Anglia, Norwich, UK, [2]Now at: School of Geography and the Environment, University of Oxford, Oxford, UK, [3]Institute of Theoretical Informatics, Karlsruhe Institute of Technology, Karlsruhe, Germany, [4]Institute of Meteorology and Climate Research (IMK-ASF), Karlsruhe Institute of Technology, Karlsruhe, Germany, [5]Department of Physics, Imperial College London, London, UK

Key Points:

- Cloud controlling factor-derived observational constraints on low and high-cloud feedback imply a higher climate sensitivity (equilibrium climate sensitivity (ECS))
- Low-cloud feedbacks drive most ECS uncertainty reduction, with high-cloud feedbacks having a secondary influence on the posterior ECS
- There is substantial dependence on the approach used to constrain the ECS on the basis of our updated cloud-feedback terms

Supporting Information:

Supporting Information may be found in the online version of this article.

Correspondence to:

S. Wilson Kemsley
s.wilson-kemsley@uea.ac.uk

Citation:

Wilson Kemsley, S., Nowack, P., & Ceppi, P. (2026). Recent cloud controlling factor analyses indicate higher climate sensitivity. *Geophysical Research Letters*, *53*, e2025GL118366. https://doi.org/10.1029/2025GL118366

Received 21 JUL 2025
Accepted 15 JAN 2026

Author Contributions:

Conceptualization: Sarah Wilson Kemsley, Peer Nowack, Paulo Ceppi
Data curation: Sarah Wilson Kemsley, Peer Nowack, Paulo Ceppi
Formal analysis: Sarah Wilson Kemsley
Funding acquisition: Peer Nowack, Paulo Ceppi
Methodology: Sarah Wilson Kemsley, Peer Nowack, Paulo Ceppi
Visualization: Sarah Wilson Kemsley
Writing – original draft: Sarah Wilson Kemsley
Writing – review & editing: Peer Nowack, Paulo Ceppi

Abstract Cloud feedback is a dominant source of uncertainty in climate model estimates of equilibrium climate sensitivity (ECS). Cloud controlling factor analysis can observationally constrain cloud feedback. For the first time, we use separate rather than unified frameworks to assess high- and low-cloud feedbacks and constrain the net cloud feedback and subsequently, the ECS. We find a robustly positive cloud feedback (i.e., a negative feedback is <0.5% probable), indicating that clouds amplify global warming. We assess the individual and combined impacts of our cloud feedback constraints on ECS using three approaches. Two indicate an upward ECS shift with reduced uncertainty, preserving ECS–feedback correlations but using cloud feedback as a single line of evidence. The third, a Bayesian framework combining multiple lines of evidence, also suggests a higher ECS but with a smaller increase and broader confidence range.

Plain Language Summary The equilibrium climate sensitivity (ECS) is a measure of the Earth's temperature response to a doubling of atmospheric carbon dioxide. However, climate model projections of the ECS remain highly uncertain. Clouds respond to CO_2-driven environmental changes (e.g., increasing surface temperature) which can amplify or dampen climate change. Such cloud feedbacks have been pinpointed as a dominant source of uncertainty in the ECS. Cloud-controlling factor analysis derives relationships between meteorological variables and clouds in an attempt to reduce uncertainties in model projections of the cloud feedback. Our separate high- and low-cloud controlling factor frameworks yield robustly positive estimates of the overall cloud feedback (with less than 0.5% probability of being negative). We subsequently evaluate the downstream constraints on the ECS, following three distinct approaches. In all cases, we find a shift toward higher values, but note that the shape of the constrained ECS distribution is strongly dependent on our prior assumptions, including the climate models considered.

1. Introduction

The equilibrium climate sensitivity (ECS), defined as the Earth's steady-state temperature response to a doubling of atmospheric carbon dioxide (CO_2), serves as a foundation for understanding the planet's response to increasing greenhouse gas emissions. Despite the increasing sophistication of the Earth System Models (ESMs) used to simulate the Earth's response to CO_2, ECS projections are still subject to considerable uncertainty (Forster et al., 2021; Marvel & Webb, 2025; Sherwood et al., 2020). In fact, the most recent Coupled Model Intercomparison Project Phase 6 (CMIP6) generation of ESMs covers a wider range of ECS estimates than previous generations, spanning 1.8–5.6 K (Zelinka et al., 2020).

Cloud feedback has been pinpointed as a prevailing cause of the uncertainty within CMIP5/6 ECS projections (Sherwood et al., 2020). As the atmosphere warms, the vertical structure, microphysics, and areal coverage of clouds changes, thus modulating the global top-of-the-atmosphere (TOA) energy balance and either amplifying or dampening climate change. Sherwood et al. (2020) identify six key mechanisms driving the net cloud feedback: reductions in the areal coverage of tropical and mid-latitude marine low clouds, tropical anvil clouds, and land clouds; increasing free-tropospheric cloud altitude; and changes in high-latitude, low-cloud optical depth.

Since Sherwood et al. (2020, hereafter S20)'s assessment, several studies have sought to improve process understanding and tighten uncertainties associated with different feedback mechanisms. For example, anvil cloud (McKim et al., 2024; Sokol et al., 2024) and tropical low-cloud (Cesana & Del Genio, 2021; Myers et al., 2021; Wu et al., 2025) feedbacks have received particular attention due to their large uncertainties. Approaches include:

constraints derived from satellite observations (Cesana & Del Genio, 2021; Raghuraman et al., 2024; Wall et al., 2022), cloud-resolving models (Sokol et al., 2024), theoretical approaches (McKim et al., 2024), emergent constraints (Thackeray et al., 2024), and cloud-controlling factor (CCF) analyses (Ceppi et al., 2024; Myers et al., 2021; Wilson Kemsley et al., 2025; Wu et al., 2025).

Here, we focus on CCF analyses given their foundation in being (a) robustly applicable across CMIP archives, (b) motivated by physical intuition in the choice of the CCFs, and (c) providing direct links between historical and future data (Nowack & Watson-Parris, 2025). CCFs are meteorological variables shaping the large-scale cloud environment and life-cycle (Andersen et al., 2023; Klein et al., 2017; Stevens & Brenguier, 2009; Wilson Kemsley et al., 2024). CCF-based observational cloud feedback constraints derive relationships between historical cloud-induced top-of-atmosphere (TOA) radiative anomalies and the CCFs. Assuming linearity, the relationships derived from historical simulations are extrapolated into and validated under warmer climates, typically using abrupt quadrupling of CO_2 (abrupt-4 $\times CO_2$) experiments across ESMs (e.g., Ceppi et al., 2024; Ceppi & Nowack, 2021; Myers et al., 2021; Qu et al., 2015; Wilson Kemsley et al., 2025). By extension, these approximately climate-invariant relationships can be estimated from observational data and used to constrain cloud-radiative responses to changes in the CCFs.

Ceppi and Nowack (2021, hereafter CN21) advanced previous frameworks by using ridge regression to derive the CCF relationships, rather than using multiple linear regression (MLR) with locally defined CCFs (e.g., Myers et al., 2021; Qu et al., 2015). CN21 showed that using CCFs within large spatial domains (instead of locally defined) increased predictive skill for global cloud feedback (λ_{NET}) under abrupt-4×CO_2 climate model projections—likely due to the synoptic scale within which the life-cycle of clouds exists in monthly-average data. More recent CCF analyses have sought to constrain feedback associated with specific cloud types or altitudes (Ceppi et al., 2024; Myers et al., 2021; Wilson Kemsley et al., 2025; Wu et al., 2025), motivated by the different processes driving feedback from different cloud regimes (Ceppi et al., 2017; Fuchs et al., 2018; Gettelman & Sherwood, 2016).

For example, Ceppi et al. (2024; hereafter C24) followed a similar approach to CN21 but for feedback specifically isolated from low clouds (λ_{LOW}). C24 used CCFs and a spatial domain optimized for the abrupt-4×CO_2 predictions of λ_{LOW} and found a more strongly amplifying feedback than most climate models suggest. Their work built upon Myers et al. (2021), who also constrained λ_{LOW} (instead using MLR with local CCFs) but found a less positive low cloud feedback. C24 showed that the discrepancy between theirs and Myers et al. (2021)'s constraint was due to the changed CCF sensitivity patterns with increased domain size, which more accurately captured the forced response.

Motivated by the uncertain anvil cloud feedback, Wilson Kemsley et al. (2025, hereafter WK25) used CCF analysis to observationally constrain feedback from changes in high-cloud amount, using CCFs and a spatial domain specifically targeting high clouds (Wilson Kemsley et al., 2024). It is considered highly likely that the areal coverage of anvil clouds decreases as the atmosphere warms (Bony et al., 2016; McKim et al., 2024; Saint-Lu et al., 2020; Wodzicki & Rapp, 2022). WK25 showed that ESMs typically underestimate these reductions in global high-cloud amount and even more substantially underestimate associated longwave (LW) and shortwave (SW) cloud feedbacks, which observations indicate are large and robustly negative and positive, respectively (also shown by Raghuraman et al., 2024). WK25 attributed this to a misrepresented "stability iris" mechanism within the climate models (Bony et al., 2016; Zelinka & Hartmann, 2010, 2011). Regardless, they found an approximately neutral high-cloud amount feedback, indicating that reductions in areal anvil cloud coverage would not drive a globally stabilizing feedback.

Recent advances in CCF analysis now allow optimized setups for constraining low- and high-cloud feedbacks, motivating us to derive distinct observational constraints for each and combine them into a joint constraint on λ_{NET}. This approach also enables us to assess, for the first time within a CCF-type framework, how constraints on high-cloud feedbacks shape downstream ECS constraints. This methodological separation aligns with the multiple lines of evidence framework of S20, treating separate cloud-feedback components as distinct yet complementary sources of information. We first use separate, targeted CCF frameworks to constrain low- and high-cloud feedbacks before deriving a joint constraint on λ_{NET}. We then evaluate how these updated cloud-feedback constraints influence ECS estimates under three distinct approaches: (a) using our λ_{NET} constraint directly, (b) applying separate high- and low-cloud feedback constraints while preserving their correlation structure, and (c) incorporating our constraints as one of several lines of evidence within S20's Bayesian framework.

2. Data and Methods

2.1. Data Sets

For observations, we use the Moderate Resolution Imaging Spectroradiometer (MODIS) combined Aqua/Terra cloud property data set, collection 6.2 (Pincus et al., 2023), from July 2002 to June 2023. In place of direct observations, ERA5 meteorological CCFs are used. For our core set of ESMs, we use 16 CMIP5/6 models that have run the International Satellite Cloud Climatology Project (ISCCP) simulator (for both historical and abrupt-4×CO_2 scenarios) and, for consistency with previous work, we use historical simulations from 1981 to 2000 (C24, WK25). We use abrupt-4×CO_2 simulations from an additional 30 ESMs where all meteorological variables required to calculate the CCFs are available (totaling 46; Text S1 in Supporting Information S1). All data sets have been re-gridded to a common 5° × 5° spatial resolution with monthly-mean temporal resolution. We use a "near-global" spatial domain from 60°S to 60°N; high latitudes are excluded because of artifacts arising at high solar zenith angles.

Both MODIS and the ISCCP CMIP5/6 data provide cloud-amount histograms, from which radiative anomalies associated with changes in clouds at different top pressures can be derived using cloud-radiative kernels (Zelinka, 2022; Zelinka et al., 2016). We isolate cloud-radiative anomalies, R, from non-low (hereafter "high" for conciseness) and low clouds, according to their cloud-top pressures. For MODIS, we follow previous studies (e.g., Ceppi et al., 2024; Myers et al., 2021; Wilson Kemsley et al., 2025; Zelinka et al., 2016) and define high clouds with top pressures <680 hPa. For the ESMs, the ISCCP simulator tends to misattribute mid-level clouds in the 560–680 hPa range to higher pressure levels (Ceppi et al., 2024) and therefore we use a lower cutoff of 560 hPa instead. All other clouds we define as low, accounting for obscuration of low-clouds by upper-level clouds following Zelinka et al. (2024). We refer to low- and high-cloud radiative anomalies as R_{LOW} and R_{HIGH}, respectively. Categorizing clouds by atmospheric pressure allows us to select CCFs targeting the different cloud types and constrain them separately. We first remove the seasonal cycles from all variables as is commonplace in these analyses (Andersen et al., 2023; Myers et al., 2021; Wilson Kemsley et al., 2024).

2.2. Statistical Framework

We first determine cloud-radiative "sensitivities" at each grid-cell, using separate frameworks for R_{LOW} and R_{HIGH}. We approximate a change in R at each grid-cell r as a linear function of anomalies in the CCFs, $\boldsymbol{X}$:

$$dR(r) \approx \sum_{i=1}^{M} \frac{\partial R(r)}{\partial \boldsymbol{X_i}} d\boldsymbol{X_i}, \tag{1}$$

for the LW and SW components of R_{HIGH} and R_{LOW}, where M is equal to the number of unique CCFs, $\boldsymbol{X}$ is a vector of length equal to the total number of surrounding grid-cells (i.e., "spatial domain") centered at grid-cell r, and the sensitivity, $\boldsymbol{\Theta}$ to the i-th CCF is defined as

$$\boldsymbol{\Theta_i} = \frac{\partial R(r)}{\partial \boldsymbol{X_i}}. \tag{2}$$

We calculate $\boldsymbol{\Theta}$ using ridge regression instead of MLR as it allows us to consider non-local CCFs within larger spatial domains with a much lower risk of over-fitting (Andersen et al., 2020, 2023; Ceppi & Nowack, 2021; Nowack et al., 2023; Wilson Kemsley et al., 2024).

Though we build on the work of C24 and WK25, we recalculate constraints on low-cloud and high-cloud feedbacks anew, maintaining consistent methodology. For low clouds, we follow C24, using: surface temperature (T_{sfc}), relative humidity at 700 hPa (RH_{700}), estimated inversion strength (EIS; over ocean, lower tropospheric stability over land), sea-surface temperature advection (SST_{adv}), near-surface wind speed (WS) and vertical velocity at 700 hPa (ω_{700}) as CCFs within a 5 × 5 grid-cell domain (corresponding to a 25° × 25° longitude ×latitude grid) for low clouds. Our key difference to C24 is our sampling of observational uncertainty from MODIS alone (see below).

For R_{HIGH}, we follow WK25's framework, though here constraining the total high-cloud feedback. We use WK25's CCFs: T_{sfc}, upper tropospheric static stability (S_{UT}), RH_{700}, upper tropospheric relative humidity

(UTRH), upper tropospheric (easterly) wind shear (ΔU_{300}), and vertical velocity at 300 hPa (ω_{300}) and a 21×11 grid-cell domain (which corresponds to a $105° \times 55°$ longitude ×latitude grid). Justifications for our choice of domain sizes and CCF calculations are provided in Text S1 of Supporting Information S1.

The CMIP5/6 sensitivities are subsequently multiplied by their corresponding ESM CCF responses to the global mean surface temperature (GMST) increase associated with abrupt-4×CO_2 experiments for each grid-cell within the spatial domain,

$$\frac{dR(r)}{d\mathrm{GMST}} \approx \sum_{i=1}^{M} \mathbf{\Theta}_i \frac{d\boldsymbol{X}_i}{d\mathrm{GMST}}, \tag{3}$$

yielding a "local feedback." We hence calculate the area-weighted mean and multiply by 0.86 to approximate a global-mean value, accounting for the fractional surface area within 60°S–60°N while neglecting contributions of the small polar regions to the global-mean feedback. This is henceforth referred to as our climate model "predicted" feedback.

We calculate the ESM "actual" feedback by regressing global-mean R (calculated within the same 60°S–60°N latitude range) against the GMST increase associated with corresponding abrupt-4×CO_2 experiments (Gregory et al., 2004) and multiplying by 0.86. We then regress the actual cloud feedback against our predicted cloud feedback to calculate the prediction error. This captures uncertainty from our choice of CCFs as well as imperfections in the linear ridge functions and their extrapolative skill under 4×CO_2 projections.

For our observational constraints, we first learn observed sensitivities (Equation 2). To quantify observational uncertainty, we follow WK25's approach and draw (with replacement) ten 20-year samples of monthly observed R (and the CCFs), thus calculating 10 sets of observational sensitivities for LW and SW R_{LOW} and R_{HIGH}. Note that we use consistent resampling indices for both high and low cloud frameworks to maintain consistency (where net feedbacks are the sum of the separate high and low feedback terms). Observational uncertainty has also been quantified using separate satellite products (without bootstrapping, e.g., CN21, C24), but it is known that several satellite data sets may suffer from artifacts arising from (e.g.) orbital drift and missing data (Norris & Evan, 2015), which WK25 found affected their constraint. Observed sensitivities are then multiplied by the 46 sets of abrupt-4×CO_2 CCF projections (Equation 3), and we use a Monte-Carlo sampling method to derive a constraint on the observational uncertainty incorporating the prediction error (Text S2 and S3 in Supporting Information S1) (Ceppi & Nowack, 2021; Nowack et al., 2023).

Finally, we constrain the ECS using our observational cloud feedback constraints, following three commonly used approaches. First, we regress the ECS for each ESM against our cloud feedback predictions (e.g., Ceppi & Nowack, 2021; Myers et al., 2021), which are well correlated due to the role clouds play in ECS uncertainty. The second approach by Bretherton and Caldwell (2020) was constructed for combining several emergent constraints. In our application, we fit a multivariate Gaussian probability density function (PDF) to the ECS and to the observationally constrained cloud feedbacks. Finally, we follow S20's Bayesian approach, which is by design not sensitive to a single line of evidence. Each approach is discussed in more detail in Sections 4.1–4.3. All uncertainties henceforth denote 90% confidence ranges, and significant correlations at the $p = 0.05$ level are denoted using an asterisk throughout the Main Text (*).

3. Cloud Feedback Constraints

We first recalculate C24's low-cloud constraint following our bootstrapping approach for the observational uncertainty. This yields a central estimate of $\lambda_{\mathrm{LOW}} = 0.46 \pm 0.16$ Wm^{-2} K^{-1}, more positive than the multi-model mean by 0.20 Wm^{-2} K^{-1} (Figure 1a). Our estimate is essentially identical to C24's of $\lambda_{\mathrm{LOW}} = 0.45 \pm 0.27$ Wm^{-2} K^{-1}, and our observationally constrained λ_{LOW} spatial distribution (Figure S2 in Supporting Information S1) qualitatively resembles C24's five-dataset constraint, reinforcing confidence in sampling from MODIS alone. Our estimate however, has a tighter confidence range; a likely consequence of sampling uncertainty within MODIS, in addition to exclusion of potential observational artifacts from alternative data sets (Norris & Evan, 2015). Our central estimate for λ_{LOW} is slightly more positive (+0.05 Wm^{-2} K^{-1}) than the sum of S20's assessed low-cloud feedbacks. Importantly, our constrained 66% confidence range corresponds to approximately a 60% reduction in uncertainty over S20. Note that here, we have split S20's assessed land-cloud feedback equally

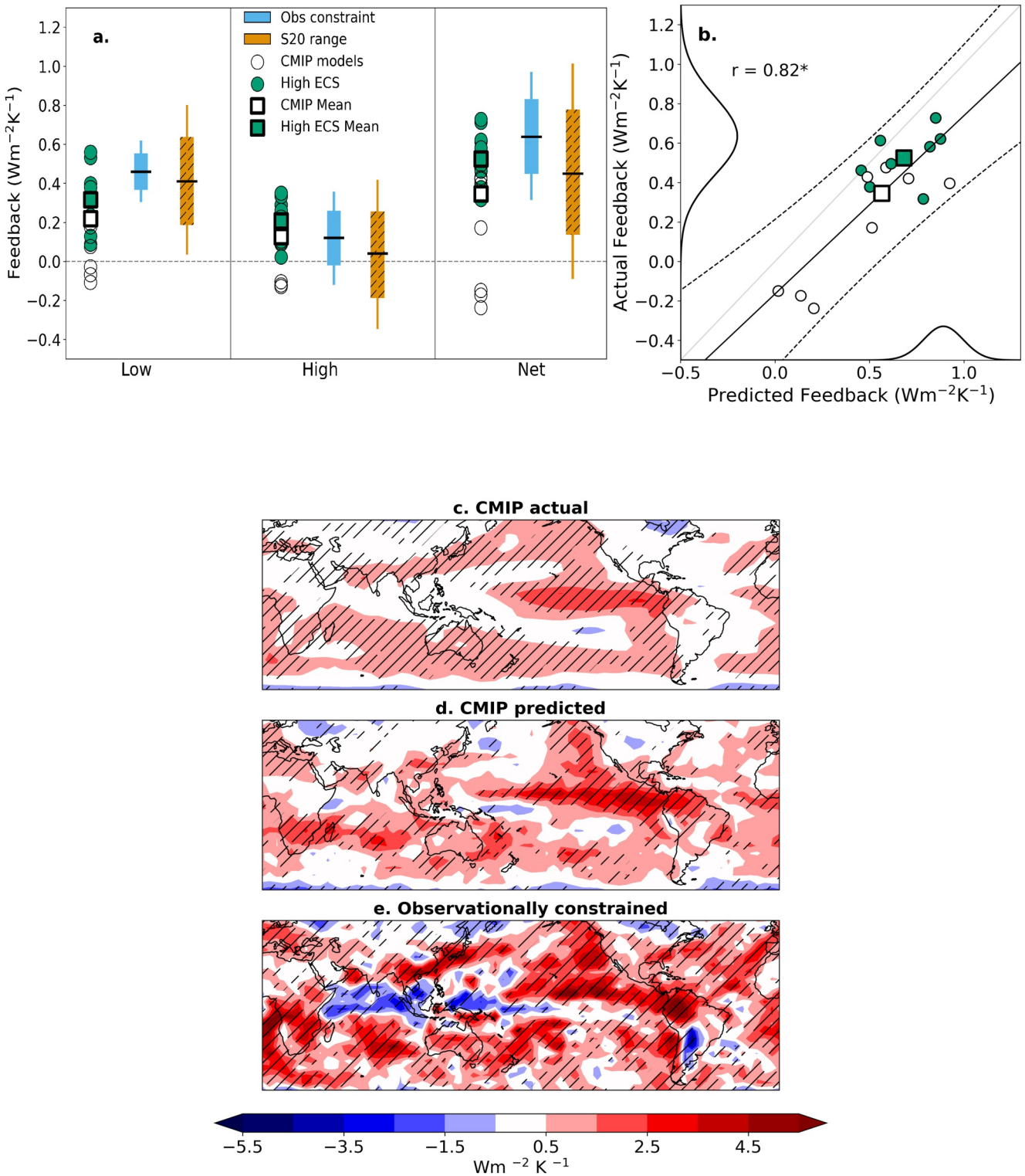

Figure 1. (a) Central estimates and uncertainty ranges for λ_{LOW}, λ_{HIGH} and λ_{NET} from ESMs, observations (solid bars), and S20 (hatched bars). Thin and thick bars are the 90% and 66% confidence ranges, respectively. (b) Actual versus predicted λ_{NET} for 16 ESMs. Solid and dashed lines are the lines-of-best-fit, and 95% prediction errors (Text S2 and S3 in Supporting Information S1), respectively (1:1 line is indicated in solid gray). Distributions on the *x*- and *y*-axis are (arbitrarily scaled) PDFs for the observational estimates. High-ECS (≥4.5 K) models are denoted using colored symbols. Multi-model mean (c) "actual" and (d) "predicted" feedback, versus (e) observationally constrained λ_{NET}. Hatching in (c–e) denotes regions where 80% of the models or observational realizations share the same sign.

into high and low-cloud feedbacks. According to S20, most of their +0.08 Wm^{-2} K^{-1} land-cloud feedback is likely due to reductions in the amount of low-level clouds (but clouds at all vertical levels decrease). If we were to ascribe all of S20's land-cloud feedback to low clouds, our central estimate is even closer to S20's (with only +0.01 Wm^{-2} K^{-1} difference).

Now constraining λ_{HIGH} (extending WK25 who only constrained the high-cloud amount feedback), we find a central estimate of 0.12 ± 0.24 Wm^{-2} K^{-1} (Figure 1a), close to the multi-model mean of 0.13 Wm^{-2} K^{-1} but more positive than S20 (by +0.08 Wm^{-2} K^{-1}). The correlations between predicted and actual LW and SW high-cloud feedback components are individually strong, but when summed, a large proportion of the variability cancels (Figure S3 in Supporting Information S1). This leaves a smaller spread in net λ_{HIGH} to constrain. Importantly, a smaller spread in ESM λ_{HIGH} does not mean the models are in agreement—several ESMs reproduce the "right" net λ_{HIGH} but for the wrong physical reasons. In the model mean, positive net λ_{HIGH} is driven by a positive LW feedback offset by a weakly negative SW feedback (Figure S3 in Supporting Information S1). In contrast, our constraint indicates an approximately neutral LW feedback and a positive SW feedback. Near-neutral LW (high-cloud) feedback likely arises from an observationally implied stronger negative feedback from global reductions in high-cloud amount (WK25), offset by a positive LW feedback from rising free-tropospheric cloud altitude (Zelinka & Hartmann, 2010). Supporting this, we find the largest discrepancies between observationally constrained and ESM feedbacks are in the tropics (Figure S2 in Supporting Information S1).

Next, we constrain λ_{NET} by summing the corresponding bootstrapped observational λ_{HIGH} and λ_{LOW} realizations (each derived from their own CCF frameworks), along with the corresponding ESM-predicted and actual feedbacks. The strong correlation between predicted and actual λ_{NET} ($r = 0.82^{*}$; Figure 1b) demonstrates that the CCF relationships remain valid when applied separately to different cloud components, also confirming their approximate invariance across climate timescales. To test whether separate frameworks improves the constraint, we repeat our analysis using a unified framework, learning sensitivities for the total LW and SW components (not partitioned by cloud-top pressure) using the same CCFs as CN21—EIS, T_{sfc}, RH_{700}, UTRH, and vertical velocity at 500 hPa within a 21 × 11 grid-cell spatial domain. Our separate frameworks yield a tighter constraint (by approximately 10%) on λ_{NET} than this unified approach (Figure S4 in Supporting Information S1). Additionally, tailored CCFs produce more physically interpretable sensitivities (not shown here; see Wilson Kemsley et al. (2024) or CN24) since high- and low-cloud feedbacks arise from distinct mechanisms (Ceppi et al., 2017; Gettelman & Sherwood, 2016; Wilson Kemsley et al., 2024).

We find a robustly positive central estimate of $\lambda_{NET} = 0.64 \pm 0.32$ Wm^{-2} K^{-1} (Figures 1a and 1b). Our central estimate lies within—though at the upper end of—the IPCC Sixth Assessment Report (AR6)'s "likely" range (0.12–0.72 Wm^{-2} K^{-1}; Forster et al., 2021), noting that our 66% upper-interval lies beyond this "likely" range. Our estimate is also more positive than the multi-model mean (+0.24 Wm^{-2} K^{-1}) and S20's central estimate (+0.19 Wm^{-2} K^{-1}), though our 90% confidence range is entirely encapsulated within S20's 90% confidence range. Our constrained 90% confidence range is approximately 30% tighter than both the ESMs and S20, and according to our constraint, negative λ_{NET} is less than 0.5% probable, despite being negative in three ESMs (none of which we consider "high-ECS" models). Our higher estimate is largely driven by λ_{LOW}, and partitioning the cloud-feedback contributions into distinct regimes (Text S4 and Figure S1 in Supporting Information S1) reveals that the discrepancy cannot be attributed to a single regime, as constraints are consistently more positive (except tropical ascent). Our central estimate is also higher than CN21's (0.43 Wm^{-2} K^{-1}). This may arise from several factors, including our subset of models, different cloud-radiative data sets, or the inclusion of all CCFs in our extrapolation.

We find that observationally-constrained and CMIP CCF-predicted spatial distributions for λ_{NET} are broadly similar, but with larger magnitudes for the former (Figures 1e and 1d). Discrepancies in sign are however present in the Eastern Pacific, Maritime Continent and Indian Ocean where observationally-derived CCFs suggest negative contributions. The close spatial agreement between the "CMIP-predicted" and "CMIP-actual" feedbacks (Figures 1c and 1d) indicates that these discrepancies are driven primarily by differences between the observed and ESM sensitivities. Examining the spatial distributions for λ_{LOW} and λ_{HIGH} reveals that this discrepancy in sign is largely due to strong negative contributions from λ_{HIGH} (Figure S2 in Supporting Information S1) which we ascribe to the ESMs underestimating decreases in high-cloud amount with warming (WK25).

4. Constraining the ECS

The ECS quantifies Earth's long-term warming response to greenhouse gas forcing and has significant policy implications (Grose et al., 2018; Hassler et al., 2018). For example, halving the uncertainty in climate sensitivity could yield global economic savings of trillions of dollars (Hope, 2015). We thus explore the implications of our cloud feedback constraints on the ECS by comparing three distinct approaches, showing that constraints differ substantially depending on prior assumptions and methodological choices. Our analysis highlights the importance of the ECS—feedback correlation structure, but also the need to constrain not only the uncertainty in cloud feedback but also its central estimate, which can influence the constrained range. Henceforth, we make a distinction between the ECS calculated from our subset of 16 ESMs, $\mathrm{ECS}_{\mathrm{sub}}$ ($\mu = 4.06 \pm 1.74$ K, $N = 16$), and the ECS for ESMs where all meteorological variables are available for the extrapolation, $\mathrm{ECS}_{\mathrm{all}}$ ($\mu = 3.48 \pm 1.64$ K, $N = 46$).

First, we follow a regression-based approach (CN21, Myers et al., 2021, C24), using our predictions for λ_{NET} (Figures 1a and 1b). We refer to this ECS constraint as $\mathrm{Regression}_{\mathrm{net}}$. Secondly, we explore Bretherton and Caldwell (2020, hereafter BC20)'s method for combining constraints using separate λ_{HIGH} and λ_{LOW} constraints. We refer to this constraint as $\mathrm{Gaussian}_{\mathrm{high-low}}$. These two approaches preserve the correlation structure between cloud feedbacks and ECS. Finally, we substitute our revised λ_{NET} estimate into S20's Bayesian framework, referring to this ECS constraint as $\mathrm{Bayesian}_{\mathrm{net}}$. Incorporating a broader range of evidence, this approach does not account for relationships between individual feedback terms and the ECS.

4.1. Regression Constraint

ECS is physically related to the effective radiative forcing, F, and the total feedback parameter, λ_{TOTAL}, which includes contributions from all sources of feedback, through $\mathrm{ECS} = -\frac{F}{\lambda_{\mathrm{TOTAL}}}$. Thus, the inverse of the ECS is also proportional to the net cloud feedback parameter. We regress $\mathrm{ECS}_{\mathrm{sub}}$ (not its reciprocal like CN21 and C24) against predicted λ_{NET}. This is to facilitate a straightforward comparison with method BC20, where ECS must be normally distributed (Text S6 in Supporting Information S1). We find that $\mathrm{ECS}_{\mathrm{sub}}$ is well correlated ($r = 0.65^{*}$) with our predictions for λ_{NET}. A key difference between this approach and BC20 is that it does not impose assumptions about the shape of the constrained ECS distribution. We find a central value for constrained $\mathrm{Regression}_{\mathrm{net}} = 4.92 \pm 1.50$ K, higher than the multi-model mean $\mathrm{ECS}_{\mathrm{sub}}$ by 0.86 K (Figure 2b) and falling above the 66% confidence range of S20's assessment and the "likely" AR6 range (Forster et al., 2021; Sherwood et al., 2020).

4.2. Gaussian Constraint

Next, we follow BC20's "Method U" for constraining the ECS using emergent, conditionally uncorrelated constraints, applied to observational constraints. We build a joint multivariate Gaussian PDF for ECS and the cloud feedback terms based on ESM-derived relationships, assuming that the ESM feedbacks, ECS, and observational errors are normally distributed (Text S5 and S6 in Supporting Information S1). Specifically, we build the multivariate PDF using two, separate feedback terms: λ_{HIGH} and λ_{LOW}.

Constraining $\mathrm{ECS}_{\mathrm{sub}}$ in this way yields a central estimate of $\mathrm{Gaussian}_{\mathrm{high-low}}$ of 4.63 ± 1.46 K; a 0.57 K increase compared to the multi-model mean $\mathrm{ECS}_{\mathrm{sub}}$ (Figure 2b). This is just under a 20% reduction in the ESM 90% confidence range and a slightly tighter constraint than $\mathrm{Regression}_{\mathrm{net}}$. The discrepancies between $\mathrm{Gaussian}_{\mathrm{high-low}}$ and $\mathrm{Regression}_{\mathrm{net}}$ arise primarily from methodological differences, but with a minor contribution from conditioning the ECS on two constraints rather than just one. For example, Figure 2c "$\mathrm{Gaussian}_{\mathrm{net}}$" shows constrained ECS only using our λ_{NET} constraint (Figure 1a), marginally wider than $\mathrm{Gaussian}_{\mathrm{high-low}}$.

$\mathrm{Gaussian}_{\mathrm{high-low}}$ is only slightly narrower than $\mathrm{Gaussian}_{\mathrm{net}}$ due to a more positive correlation between the ESM $\mathrm{ECS}_{\mathrm{sub}}$ and λ_{NET} distributions ($r = 0.83^{*}$; note that the correlation shown in Figure 2a is between *predicted* λ_{NET} and ECS) than between $\mathrm{ECS}_{\mathrm{sub}}$ and λ_{LOW} or λ_{HIGH} ($r = 0.75^{*}$ and $r = 0.59^{*}$, respectively). $\mathrm{Gaussian}_{\mathrm{high-low}}$, however, yields intuitive weights linking each term to the constrained mean ECS,

$$\Delta \approx 0.11 \times \bar{x}_{\mathrm{o,HIGH}} + 0.38 \times \bar{x}_{\mathrm{o,LOW}}, \tag{4}$$

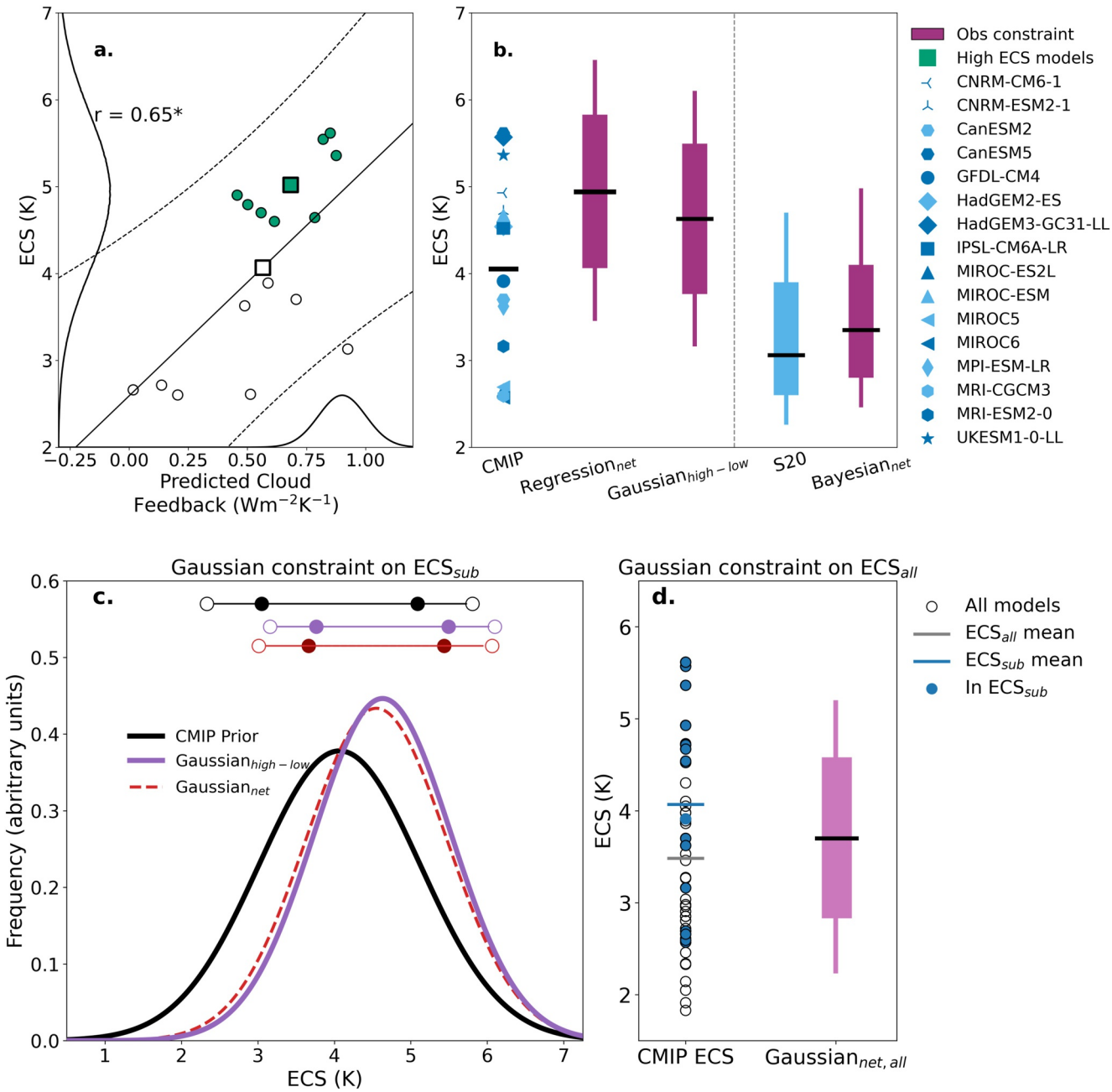

Figure 2. (a) ECS_{sub} against predicted λ_{NET}. (b) Observational constraint on ECS_{sub} derived using panel (a) ($Regression_{net}$), the Gaussian constraint ($Gaussian_{high-low}$), alongside S20's equilibrium climate sensitivity distribution and "$Bayesian_{net}$." (c) The CMIP Prior and Gaussian constraints on ECS_{sub} ("$Gaussian_{high-low}$" and "$Gaussian_{net}$"). Circles (empty and solid) above PDFs show 90% and 66% confidence ranges, respectively. (d) Gaussian constraint on ECS_{all}, derived from 46 climate models and our λ_{NET} (Figure 1a). Thin and thick rectangles in all panels denote the 90% and 66% confidence ranges, respectively.

where $\bar{x}_{o,HIGH}$ and $\bar{x}_{o,LOW}$ represent how strongly the central estimates of our high- and low-cloud feedback constraints deviate from the ESM means (Text S5 in Supporting Information S1), which we use to quantify the separate impacts of the λ_{LOW} and λ_{HIGH} constraints on $Gaussian_{high-low}$. The weight for $\bar{x}_{o,LOW}$ is larger than $\bar{x}_{o,HIGH}$ due to the dominant role of low-cloud feedbacks in driving ECS uncertainty (Bony & Dufresne, 2005; Caldwell et al., 2016; Sherwood et al., 2020). Though the high-cloud weight is non-zero, its influence is small because $\bar{x}_{o,HIGH}$ deviates only slightly from the ESM mean (−0.04 weighted by 0.11; Figure S6 in Supporting Information S1), whereas $\bar{x}_{o,LOW}$ deviates more strongly (+1.07, weighted by 0.38). Despite contributing little to

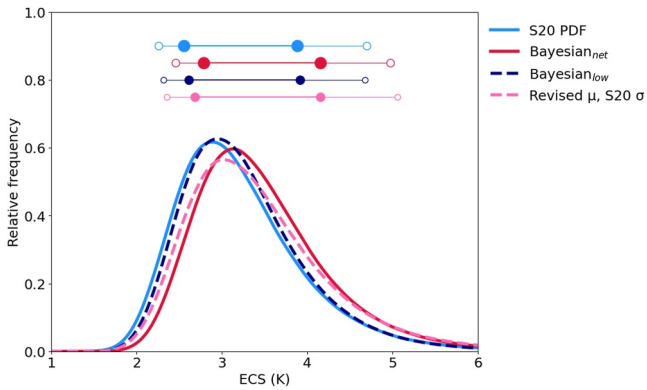

Figure 3. Sherwood et al. (2020)'s equilibrium climate sensitivity probability density function ("S20 PDF"), our constraint using λ_{NET} ("Bayesian$_{net}$"), and λ_{LOW} only ("Bayesian$_{low}$"), and a constraint using our central estimate for λ_{NET}, but S20's uncertainty ("Revised μ, S20 σ"). Empty and filled circles above the PDFs show the 90% and 66% confidence ranges, respectively.

the upwards shift, our constraint on λ_{HIGH} explains roughly 16% as much of the posterior ECS variance reduction as λ_{LOW}.

Here, constrained ECS is sensitive to the ESM set by design, and with only 16 (high-ECS biased) ESMs, we compare our Gaussian$_{high-low}$ constraint to one derived from a more comprehensive set of ESMs (Gaussian$_{net,all}$). More ESMs have simulated the required abrupt-4×CO_2 experiments to calculate λ_{NET} (not decomposed by cloud-type; CN21), and thus we derive the joint PDF from ECS$_{all}$ ($N = 46$) and λ_{NET}, using our constrainet on λ_{NET} (Figure 1a). This yields a revised Gaussian$_{net,all}$ of 3.70 ± 1.48 K–a 0.22 K increase in the mean relative to ECS$_{all}$, and a tighter 90% confidence range by 0.32 K (Figure 2d). This is a smaller upward shift than Gaussian$_{high-low}$, primarily due to a smaller difference between the observationally constrained central estimate for λ_{NET} and the ESM mean (Figure S6 in Supporting Information S1), but also slightly smaller constraint weights due to a less positive correlation between λ_{NET} and ECS$_{all}$ ($r = 0.70^{*}$). This confirms the Gaussian constraint is highly sensitive to the set of ESMs from which the ECS prior is derived. Regardless, our finding of a warmer ECS remains consistent.

4.3. Bayesian Constraint

Both Regression$_{net}$ and Gaussian$_{high-low}$ require ESM distributions for their constraints, and therefore constrained PDFs are—at minimum, somewhat—dependent on the subset of ESMs. Our ECS$_{sub}$ is high-shifted and, due to the relatively small sample size, correlations between cloud feedback and ECS$_{sub}$ may not be fully representative of the true relationships. Furthermore, Sherwood and Forest (2024) caution that an ECS constraint based solely on ESMs may not be realistic due to shared errors within the models, and that individual cloud-feedback constraints may over-interpret downstream ECS constraints. S20 instead constrain ECS using a Bayesian framework incorporating multiple lines of evidence, including historical and paleoclimate records alongside process understanding from cloud and other climate feedbacks. However, the final ECS constraint remains subject to methodological choices that influence the shape of the constrained PDF (S20; Sherwood & Forest, 2024)

We substitute our $\lambda_{NET} = 0.64 \pm 0.32$ Wm^{-2} K^{-1} into S20's framework (S20's $\lambda_{NET} = 0.45 \pm 0.54$ Wm^{-2} K^{-1}). The revised ECS, Bayesian$_{net}$, has a central estimate of 3.35 K, an increase of 0.24 K (Figure 3). However, despite an uncertainty reduction of $\frac{1}{3}$ in λ_{NET} compared to S20, we find a widening of the updated ECS 90% confidence range, contrasting our previous approaches. Indeed, S20's 90% confidence range is 2.26–4.70 K (2.44 K width) while our Bayesian$_{net}$ 90% confidence range is 2.46–4.98 K (2.52 K width). This is due to the inverse relationship between ECS and λ, highlighting the sensitivity of the ECS uncertainty to not only the uncertainty in cloud feedback, but also its central value.

High-cloud feedback had a smaller (non-negligible) influence on Gaussian$_{high-low}$ than our low-cloud feedback constraint. We again assess the relative importance of the two feedback terms by repeating S20's Bayesian constraint without our λ_{HIGH} estimate. Combining S20's high-cloud feedback with our λ_{LOW} (adding errors in quadrature) gives $\lambda_{NET} = 0.49 \pm 0.41$ Wm^{-2} K^{-1}. Despite reduced cloud-feedback uncertainty, the newly constrained PDF ("Bayesian$_{low}$," Figure 3) remains similar to S20's original due to the less uncertain, but more positive λ_{NET}. This highlights the importance of also incorporating revised high-cloud feedback estimates into such ECS constraints.

Finally, by repeating this constraint using *our* central estimate for λ_{NET} but with S20's original uncertainty (e.g., $\lambda_{NET} = 0.64 \pm 0.54$ Wm^{-2} K^{-1}), we quantify the effect reduced uncertainty has at our more positive cloud feedback. This yields an ECS with central estimate of 3.30 K and a 90% confidence range of 2.36–5.05 K (2.69 K width) in contrast to Bayesian$_{net}$'s 2.52 K width, confirming that the original widening of uncertainty is due to the more positive λ_{NET}. A smaller tightening of the 90% confidence range (<10%) at the revised mean λ_{NET} is likely because cloud feedback is one line of evidence among many, but also the correlation structure between the ECS and specific cloud-feedbacks are not preserved. For example, ECS spread is more strongly related to λ_{LOW} than to tropical high-cloud amount feedbacks (Dawson & Schiro, 2024). Reducing the uncertainty in total λ_{NET} will not

reflect the relative strengths of these relationships. Further exploration of ECS constraints that retain the correlation structure between ECS and individual feedbacks is an avenue for future work.

5. Conclusion

We, for the first time, observationally constrain global cloud feedback (λ_{NET}) using separate CCF frameworks for high and low clouds to better represent their different physical drivers. Our observational constraint indicates a robustly amplifying global cloud feedback of 0.64 ± 0.32 Wm^{-2} K^{-1} (with <0.5% probability of being negative), more positive than the multi-model mean based on 16 climate models. This is also more positive than both Sherwood et al. (2020) and the latest IPCC report (Forster et al., 2021) central estimates, but lies within the 66% confidence and "likely" ranges of both, respectively.

Quantifying the implications of our cloud feedback constraints on the ECS following three different approaches, we find that two approaches suggest a substantial upwards shift in the climate model ECS distribution, accompanied by reductions in uncertainty. We show that the tightening of the climate model ECS posterior is mainly driven by reduced uncertainty in low-cloud feedback, but with high-cloud feedback making a non-negligible, secondary contribution. The third, following the Bayesian Sherwood et al. (2020) framework, also indicates a warmer ECS but, despite reducing cloud feedback uncertainty by approximately $\frac{1}{3}$, we find an increase in the ECS 90% confidence range. This results from our more positive cloud feedback relative to S20—driven by both low- and high-clouds, here with a slightly stronger high-cloud influence—and from the inverse relationship between ECS and cloud feedback. This highlights that ECS uncertainty depends not only on feedback uncertainty but also on its central value.

Each method provides unique benefits. The regression approach does not impose a strict normal distribution on the constrained ECS, while we can compare relative contributions of our feedback terms using the multivariate Gaussian approach. These approaches preserve the correlation structure of ECS and cloud feedback terms, though both methods use cloud feedbacks as a single indicator of ECS uncertainty, possibly overstating the downstream constraint on the ECS, and are sensitive to the underlying ESMs. Instead, S20 considers cloud feedback among other lines of evidence, and accordingly we find (keeping the central estimate for cloud feedback fixed), a smaller reduction in ECS uncertainty. Ultimately, irrespective of the ESM prior or assumptions imposed on the feedback or ECS distributions, our CCF-derived constraints consistently suggest that cloud feedback is more strongly amplifying than these climate models, S20, and the IPCC suggest.

Conflict of Interest

The authors declare no conflicts of interest relevant to this study.

Data Availability Statement

All data used in this research is freely available. ERA5 meteorological reanalysis data are from the Copernicus Climate Change Service (Hersbach et al., 2023a, 2023b). Combined MODIS Aqua–Terra data are freely available and downloaded with monthly resolution (NASA, 2022). CMIP5/6 data are obtained from the UK Center for Environmental Data Analysis portal (CEDA). Cloud radiative kernels are freely available at Zelinka (2022), and cloud-radiative sensitivities were calculated using code adapted from Nowack (2021). We used ECS values from Zelinka (2024). Code for reproducing Sherwood et al. (2020)'s Bayesian analysis was taken from Webb (2022).

Acknowledgments

We would like to thank Lina Rennstich for her technical support and the two anonymous reviewers for their constructive comments that helped improve this manuscript. This research has been supported by the UK Natural Environment Research Council, Grant NE/V012045/1 (SWK, PN, PC), NE/T006250/1 (PC) and the UK Government's Horizon Europe Funding Gaurantee, Grant EP/Y036123/1 (PC, PN). This research was carried out on the High Performance Computing Cluster supported by the Research and Specialist Computing Support service at the University of East Anglia and JASMIN, the UK's collaborative data analysis environment (https://jasmin.ac.uk). We acknowledge the World Climate Research Programme's Working Group on Coupled Modeling, which is responsible for CMIP, and we thank the climate modeling groups for producing and making available their model output. We also thank the Earth System Grid Federation (ESGF) for archiving the model output and providing access, and we thank the multiple funding agencies who support CMIP and ESGF.

References

Andersen, H., Cermak, J., Douglas, A., Myers, T. A., Nowack, P., Stier, P., et al. (2023). Sensitivities of cloud radiative effects to large-scale meteorology and aerosols from global observations. *Atmospheric Chemistry and Physics*, *23*(18), 10775–10794. https://doi.org/10.5194/acp-23-10775-2023

Andersen, H., Cermak, J., Fuchs, J., Knippertz, P., Gaetani, M., Quinting, J., et al. (2020). Synoptic-scale controls of fog and low-cloud variability in the Namib Desert. *Atmospheric Chemistry and Physics*, *20*(6), 3415–3438. https://doi.org/10.5194/acp-20-3415-2020

Bony, S., & Dufresne, J.-L. (2005). Marine boundary layer clouds at the heart of tropical cloud feedback uncertainties in climate models. *Geophysical Research Letters*, *32*(20). https://doi.org/10.1029/2005GL023851

Bony, S., Stevens, B., Coppin, D., Becker, T., Reed, K. A., Voigt, A., & Medeiros, B. (2016). Thermodynamic control of anvil cloud amount. *Proceedings of the National Academy of Sciences*, *113*(32), 8927–8932. https://doi.org/10.1073/pnas.1601472113

Bretherton, C. S., & Caldwell, P. M. (2020). Combining emergent constraints for climate sensitivity. *Journal of Climate*, *33*(17), 7413–7430. https://doi.org/10.1175/JCLI-D-19-0911.1

Caldwell, P. M., Zelinka, M. D., Taylor, K. E., & Marvel, K. (2016). Quantifying the sources of intermodel spread in equilibrium climate sensitivity. *Journal of Climate*, *29*(2), 513–524. https://doi.org/10.1175/JCLI-D-15-0352.1

Ceppi, P., Brient, F., Zelinka, M. D., & Hartmann, D. L. (2017). Cloud feedback mechanisms and their representation in global climate models. *WIREs Climate Change*, *8*(4), e465. https://doi.org/10.1002/wcc.465

Ceppi, P., Myers, T. A., Nowack, P., Wall, C. J., & Zelinka, M. D. (2024). Implications of a pervasive climate model bias for low-cloud feedback. *Geophysical Research Letters*, *51*(20), e2024GL110525. https://doi.org/10.1029/2024GL110525

Ceppi, P., & Nowack, P. (2021). Observational evidence that cloud feedback amplifies global warming. *Proceedings of the National Academy of Sciences*, *118*(30), e2026290118. https://doi.org/10.1073/pnas.2026290118

Cesana, G. V., & Del Genio, A. D. (2021). Observational constraint on cloud feedbacks suggests moderate climate sensitivity. *Nature Climate Change*, *11*(3), 213–218. https://doi.org/10.1038/s41558-020-00970-y

Dawson, E., & Schiro, K. A. (2024). Tropical high cloud feedback relationships to climate sensitivity. *Journal of Climate*, *38*(2), 583–596. https://doi.org/10.1175/JCLI-D-24-0218.1

Forster, P., Storelvmo, K., Armour, K., Collins, W., Dufresne, J.-L., Frame, D., et al. (2021). The earth's energy budget, climate feedbacks, and climate sensitivity. In P. Zhai, A. Pirani, S. L. Connors, C. Péan, S. Berger, N. Caud, Y. Chen, L. Goldfarb, M. I. Gomis, M. Huang, K. Leitzell, E. Lonnoy, J. B. R. Matthews, T. K. Maycock, T. Waterfield, O. Yelekçi, R. Yu, & B. Zhou (Eds.), *Climate change 2021: The physical science basis. Contribution of working group I to the sixth assessment report of the intergovernmental panel on climate change Masson-Delmotte* (1st ed., pp. 923–1054). Cambridge University Press. https://doi.org/10.1017/9781009157896.009

Fuchs, J., Cermak, J., & Andersen, H. (2018). Building a cloud in the southeast Atlantic: Understanding low-cloud controls based on satellite observations with machine learning. *Atmospheric Chemistry and Physics*, *18*(22), 16537–16552. https://doi.org/10.5194/acp-18-16537-2018

Gettelman, A., & Sherwood, S. C. (2016). Processes responsible for cloud feedback. *Current Climate Change Reports*, *2*(4), 179–189. https://doi.org/10.1007/s40641-016-0052-8

Gregory, J. M., Ingram, W. J., Palmer, M. A., Jones, G. S., Stott, P. A., Thorpe, R. B., et al. (2004). A new method for diagnosing radiative forcing and climate sensitivity. *Geophysical Research Letters*, *31*(3). https://doi.org/10.1029/2003GL018747

Grose, M. R., Gregory, J., Colman, R., & Andrews, T. (2018). What climate sensitivity index is Most useful for projections? *Geophysical Research Letters*, *45*(3), 1559–1566. https://doi.org/10.1002/2017GL075742

Hassler, J., Krusell, P., & Olovsson, C. (2018). The consequences of uncertainty: Climate sensitivity and economic sensitivity to the climate. *Annual Review of Economics*, *10*(1), 189–205. https://doi.org/10.1146/annurev-economics-080217-053229

Hersbach, H., Bell, B., Berrisford, P., Biavati, G., Horányi, A., Muñoz Sabater, J., et al. (2023a). ERA5 hourly data on pressure levels from 1940 to present [Dataset]. *Copernicus Climate Change Service (C3S) Climate Data Store (CDS)*. https://doi.org/10.24381/cds.bd0915c6

Hersbach, H., Bell, B., Berrisford, P., Biavati, G., Horányi, A., Muñoz Sabater, J., et al. (2023b). ERA5 monthly averaged data on pressure levels from 1940 to present [Dataset]. *Copernicus Climate Change Service (C3S) Climate Data Store (CDS)*. https://doi.org/10.24381/cds.bd0915c6

Hope, C. (2015). The $10 trillion value of better information about the transient climate response. *Philosophical Transactions of the Royal Society A: Mathematical, Physical and Engineering Sciences*, *373*(2054), 20140429. https://doi.org/10.1098/rsta.2014.0429

Klein, S. A., Hall, A., Norris, J. R., & Pincus, R. (2017). Low-cloud feedbacks from cloud-controlling factors. *A Review*, *38*(6), 1307–1329. https://doi.org/10.1007/s10712-017-9433-3

Marvel, K., & Webb, M. (2025). Towards robust community assessments of the Earth's climate sensitivity. *Earth System Dynamics*, *16*(1), 317–332. https://doi.org/10.5194/esd-16-317-2025

McKim, B., Bony, S., & Dufresne, J.-L. (2024). Weak anvil cloud area feedback suggested by physical and observational constraints. *Nature Geoscience*, *17*(5), 1–6. https://doi.org/10.1038/s41561-024-01414-4

Myers, T. A., Scott, R. C., Zelinka, M. D., Klein, S. A., Norris, J. R., & Caldwell, P. M. (2021). Observational constraints on low cloud feedback reduce uncertainty of climate sensitivity. *Nature Climate Change*, *11*(6), 501–507. https://doi.org/10.1038/s41558-021-01039-0

NASA. (2022). MODIS (Aqua/Terra) cloud properties level 3 monthly, 1 × 1 degree grid [Dataset]. https://doi.org/10.5067/MODIS/MCD06COSP_M3_MODIS.062

Norris, J. R., & Evan, A. T. (2015). Empirical removal of artifacts from the ISCCP and PATMOS-x satellite cloud records. *Journal of Atmospheric and Oceanic Technology*, *32*(4), 691–702. https://doi.org/10.1175/JTECH-D-14-00058.1

Nowack, P. (2021). Example ridge regression code in support of the publication "Observational evidence that cloud feedback amplifies global warming" by Ceppi Nowack in PNAS (2021). *GitHub*. Retrieved from https://github.com/peernow/PNAS2021

Nowack, P., Ceppi, P., Davis, S. M., Chiodo, G., Ball, W., Diallo, M. A., et al. (2023). Response of stratospheric water vapour to warming constrained by satellite observations. *Nature Geoscience*, *16*(7), 577–583. https://doi.org/10.1038/s41561-023-01183-6

Nowack, P., & Watson-Parris, D. (2025). Opinion: Why all emergent constraints are wrong but some are useful – A machine learning perspective. *Atmospheric Chemistry and Physics*, *25*(4), 2365–2384. https://doi.org/10.5194/acp-25-2365-2025

Pincus, R., Hubanks, P. A., Platnick, S., Meyer, K., Holz, R. E., Botambekov, D., & Wall, C. J. (2023). Updated observations of clouds by MODIS for global model assessment. *Earth System Science Data*, *15*(6), 2483–2497. https://doi.org/10.5194/essd-15-2483-2023

Qu, X., Hall, A., Klein, S. A., & DeAngelis, A. M. (2015). Positive tropical marine low-cloud cover feedback inferred from cloud-controlling factors. *Geophysical Research Letters*, *42*(18), 7767–7775. https://doi.org/10.1002/2015GL065627

Raghuraman, S. P., Medeiros, B., & Gettelman, A. (2024). Observational quantification of tropical high cloud changes and feedbacks. *Journal of Geophysical Research: Atmospheres*, *129*(7), e2023JD039364. https://doi.org/10.1029/2023JD039364

Saint-Lu, M., Bony, S., & Dufresne, J.-L. (2020). Observational evidence for a stability iris effect in the tropics. *Geophysical Research Letters*, *47*(14). https://doi.org/10.1029/2020GL089059

Sherwood, S. C., & Forest, C. E. (2024). Opinion: Can uncertainty in climate sensitivity be narrowed further? *Atmospheric Chemistry and Physics*, *24*(4), 2679–2686. https://doi.org/10.5194/acp-24-2679-2024

Sherwood, S. C., Webb, M. J., Annan, J. D., Armour, K. C., Forster, P. M., Hargreaves, J. C., et al. (2020). An assessment of earth's climate sensitivity using multiple lines of evidence. *Reviews of Geophysics*, *58*(4), e2019RG000678. https://doi.org/10.1029/2019RG000678

Sokol, A. B., Wall, C. J., & Hartmann, D. L. (2024). Greater climate sensitivity implied by anvil cloud thinning. *Nature Geoscience*, *17*(5), 398–403. https://doi.org/10.1038/s41561-024-01420-6

Stevens, B., & Brenguier, J.-L. (2009). Cloud controlling factors — Low clouds. In J. Heintzenberg & R. J. Charlson (Eds.), *Clouds in the perturbed climate system: Their relationship to energy balance, atmospheric dynamics, and Precipitation* (pp. 173–196). MIT Press.

Thackeray, C. W., Zelinka, M. D., Norris, J., Hall, A., & Po-Chedley, S. (2024). Relationship between tropical cloud feedback and climatological bias in clouds. *Geophysical Research Letters*, *51*(24), e2024GL111347. https://doi.org/10.1029/2024GL111347

Wall, C. J., Storelvmo, T., Norris, J. R., & Tan, I. (2022). Observational constraints on Southern Ocean cloud-phase feedback. *Journal of Climate*, *35*(15), 5087–5102. https://doi.org/10.1175/JCLI-D-21-0812.1

Webb, M. (2022). Code and data for WCRP climate sensitivity assessment (corrected version, December 2022) (version CorrectionDec2022). *Zenodo*. https://doi.org/10.5281/zenodo.7448497

Wilson Kemsley, S., Ceppi, P., Andersen, H., Cermak, J., Stier, P., & Nowack, P. (2024). A systematic evaluation of high-cloud controlling factors. *Atmospheric Chemistry and Physics*, *24*(14), 8295–8316. https://doi.org/10.5194/acp-24-8295-2024

Wilson Kemsley, S., Nowack, P., & Ceppi, P. (2025). Climate models underestimate global decreases in high-cloud amount with warming. *Geophysical Research Letters*, *52*(7), e2024GL113316. https://doi.org/10.1029/2024GL113316

Wodzicki, K. R., & Rapp, A. D. (2022). More intense, organized deep convection with shrinking tropical ascent regions. *Geophysical Research Letters*, *49*(15), e2022GL098615. https://doi.org/10.1029/2022GL098615

Wu, M., Su, H., & Neelin, J. D. (2025). Multi-objective observational constraint of tropical Atlantic and Pacific low-cloud variability narrows uncertainty in cloud feedback. *Nature Communications*, *16*(1), 218. https://doi.org/10.1038/s41467-024-53985-w

Zelinka, M. D. (2022). mzelinka/cmip56_forcing_feedback_ecs: Jun 15, 2022 release (v2.2) [Dataset]. *Zenodo*. https://doi.org/10.5281/zenodo.6647291

Zelinka, M. D. (2024). mzelinka/cloud-radiative-kernels: Sep 4, 2024 release [Dataset]. *Zenodo*. https://doi.org/10.5281/zenodo.13686878

Zelinka, M. D., Chao, L., Myers, T., Qin, Y., & Klein, S. (2024). Technical note: Recommendations for diagnosing cloud feedbacks and rapid cloud adjustments using cloud radiative kernels. *EGUsphere*, 1–27. https://doi.org/10.5194/egusphere-2024-2782

Zelinka, M. D., & Hartmann, D. L. (2010). Why is longwave cloud feedback positive? *Journal of Geophysical Research*, *115*(D16), D16117. https://doi.org/10.1029/2010JD013817

Zelinka, M. D., & Hartmann, D. L. (2011). The observed sensitivity of high clouds to mean surface temperature anomalies in the tropics. *Journal of Geophysical Research*, *116*(D23). https://doi.org/10.1029/2011JD016459

Zelinka, M. D., Myers, T. A., McCoy, D. T., Po-Chedley, S., Caldwell, P. M., Ceppi, P., et al. (2020). Causes of higher climate sensitivity in CMIP6 models. *Geophysical Research Letters*, *47*(1), e2019GL085782. https://doi.org/10.1029/2019GL085782

Zelinka, M. D., Zhou, C., & Klein, S. (2016). Insights from a refined decomposition of cloud feedbacks. *Geophysical Research Letters*, *43*(17), 9259–9269. https://doi.org/10.1002/2016GL069917

References From the Supporting Information

Chakraborty, S., Fu, R., Massie, S. T., & Stephens, G. (2016). Relative influence of meteorological conditions and aerosols on the lifetime of mesoscale convective systems. *Proceedings of the National Academy of Sciences*, *113*(27), 7426–7431. https://doi.org/10.1073/pnas.1601935113

Medeiros, B., & Stevens, B. (2011). Revealing differences in GCM representations of low clouds. *Climate Dynamics*, *36*(1), 385–399. https://doi.org/10.1007/s00382-009-0694-5

Reichler, T., Dameris, M., & Sausen, R. (2003). Determining the tropopause height from gridded data. *Geophysical Research Letters*, *30*(20). https://doi.org/10.1029/2003GL018240

Wood, R., & Bretherton, C. S. (2006). On the relationship between stratiform low cloud cover and lower-tropospheric stability. *Journal of Climate*, *19*(24), 6425–6432. https://doi.org/10.1175/JCLI3988.1